

NUMERICAL SIMULATION OF GAS-SOLID FLOW IN AN INTERCONNECTED FLUIDIZED BED

by

Giuseppe CANNETO, Cesare FREDA, and Giacobbe BRACCIO

Italian National Agency for New Technologies, Energy and Sustainable Economic Development,
UTTRI-BIOM, Laboratory of Technology and Equipment for Bioenergy and Solar Thermal,
Rotondella, Matera, Italy

Original scientific paper
DOI: 10.2298/TSCI121220002C

The gas-particles flow in an interconnected bubbling fluidized cold model is simulated using a commercial CFD package by Ansys. Conservation equations of mass and momentum are solved using the Eulerian granular multiphase model. Bubbles formation and their paths are analyzed to investigate the behaviour of the bed at different gas velocities. Experimental tests, carried out by the cold model, are compared with simulation runs to study the fluidization quality and to estimate the circulation of solid particles in the bed.

Key words: *biomass gasification, interconnected fluidized bed, two-phase flow, Eulerian*

Introduction

Biomass has been recognized as a valid contribute to the solution of world energetic problem [1]. Among the current biomass technologies, gasification is an important process to convert almost any kind of biomass to combustibles gas, useful to generate heat, power, and chemicals. In the biomass gasification field, bubbling fluidized bed (BFB) are key reactors [2].

In a typical BFB, during gasification process, the biomass, because of its lower density compared to the mineral sand, floats on the top surface of the bed; this behaviour causes elutriation phenomena of the fine carbonaceous particles in the syngas, decreasing the gasification yield. Moreover, the difficulty in maintaining the particles of biomass inside of the bed affects the good performance of gasification. The surface conditions (temperature, heat transfer and solid-gas contact) are less advantageous than those in the bed in reference to the reactions kinetics of char gasification and tars conversion. It is demonstrated that the use of a particular geometric shape of the reactor, that allows the movement of the solid material inside the bed, could overcome these disadvantages. Cold models are powerful tool to explore the hydrodynamics behaviour of the granular bed of a reactor.

Kuramoto *et al.* [3, 4] in their works used, for example, an interconnected fluidized bed (IFB) having the aim to improve the movement of the solid material inside the bed. In particular, the devices used by Kuramoto in his experimental tests, were formed by two or four fluidized chambers (see fig. 1) separated by orthogonal plates of different height and intercon-

* Corresponding author; e-mail: giuseppe.canneto@enea.it

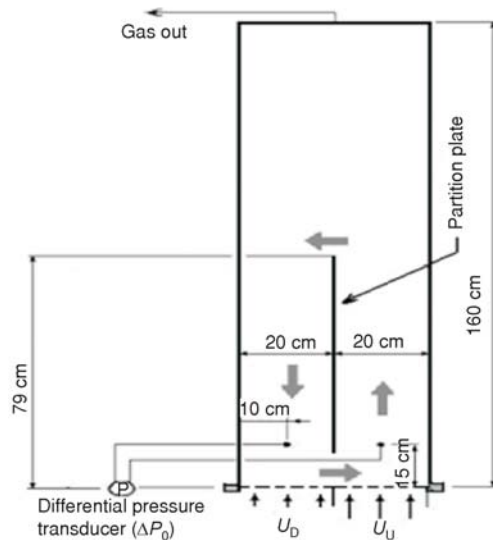


Figure 1. Scheme of two beds cold model used by Kuramoto *et al.* [4]

connected by orifices at the bottom of the plates. More recently, similar devices were, also, used by Abellon *et al.* [5] to determine the residence times of glass beads in a four-compartment interconnected fluidized bed and by Snieders *et al.* [6] to test the circulation of pellets. In all these kinds of devices, if the height of the bed is equal or higher than the height of the vertical plate, the mineral bed particles flow from the denser chamber to the other chamber through the bottom orifice, and from the less dense chamber to the other jumping the separating plate. In general the circulation of the granular material promoted by the difference of the fluidization velocities on both sides of the vertical plate, allows a good distribution of biomass particles, avoids their segregation to the surface of bed and reduces the elutriation.

Understanding particles mixing and segregation and bubble formation inside the reactor, would be useful in the design and operation of

BFB. But hydrodynamics behavior of these reactors remains complex and for some technical issues no unifying theory exists, but only empirical equations. So, numerical solution should be considered, as a useful tool, for getting inside these phenomena.

In a computational fluid dynamics (CFD) model, simplified equations, derived from the basic principles of conservation of mass, momentum, energy, and chemical species, are used. These, together with the boundary conditions, constitutive relationships and thermodynamics data give the flow fields at discrete points in the calculation domain.

Aim of the present work is to assess the capability of a numerical simulation in a 2-D frame to simulate the hydrodynamics of an interconnected fluidized bed (IFB) cold flow model. In addition, the paper focuses on the measure of the circulation of solid material in the bed, comparing the simulations runs and the experimental tests executed by the cold model.

Gas-solid multiphase model

Two classes of models can be considered in the area of gas-solid hydrodynamics modeling: Eulerian-Lagrangian models and Eulerian-Eulerian models. The first class of models can solve the equations of motion for each individual particle. Being highly time consuming, these models are generally used in systems containing a limited number of particles. Eulerian-Eulerian approach, instead, treats the particles as a continuum too, and considers the two phases forming two interpenetrating continuum media. The approach requires closure equations both for the fluid-solid and solid-solid momentum transfer and both for fluid and solid phase stress tensors.

In general in a gas-solid system, the mechanisms and formulation of interaction forces have been investigated, starting from studies on the dynamics of a single particle, by many authors [7-10]. Among the different mechanisms of interactions, the most significant forces (buoyancy and drag force) are, in many cases, the only considered ones since satisfactory formulations of the other effects do not exist. At the same time, the choice of the model for stresses term

that must be considered in the particulate momentum equation is a matter of discussion. In fact, in a fluidized bed the particles are in permanent contact in very dense regions (high solid volume fraction), where there is prevalence of frictional stresses, and are in collisional contact in the dilute regions (low solid volume fraction) where there is prevalence of kinetic stresses. In the transition regions the frictional stresses and kinetic stresses can be both important. The kinetic theory of granular flow (KTGF) is used to model the kinetic stresses and is generally accepted. To describe the stresses in the plastic regime some theories derived from soil mechanics have been proposed. Instead, there is no generally accepted theory for the intermediate regime. For this latter regime it was proposed to combine the two theories for the kinetic and for the plastic stresses [11].

Governing and constitutive equations used by the code

In Fluent (Ansys FluentTM ver.12.1), the Eulerian multi-fluid granular model treats the different phases mathematically as interpenetrating continua and solves the momentum and the volume fraction equations for each phase. The derivation of the conservation equations can be done by averaging the local instantaneous balance for each of the phases. The volume fractions, are assumed to be continuous functions of space and time. In the following, with the hypothesis of absence of species transport and chemical reactions, equations of conservation for the mass and momentum for the two phases and closure laws used in the code are briefly described [12].

The conservation of mass for the generic phase q (gas or solid) is:

$$\frac{\partial(\rho_q \varepsilon_q)}{\partial t} + \nabla(\rho_q \varepsilon_q \vec{v}_q) = 0 \quad (1)$$

with the constrain $\sum \varepsilon_q = 1$.

In general the conservation of momentum equation for a fluid phase, has the following form:

$$\frac{\partial(\rho_g \varepsilon_g \vec{v}_g)}{\partial t} + \nabla(\rho_g \varepsilon_g \vec{v}_g \vec{v}_g) = -\varepsilon_g \nabla p + \nabla \bar{\bar{\tau}}_g + \varepsilon_g \rho_g \vec{g} + K(\vec{v}_s - \vec{v}_g) \quad (2)$$

where

$$\bar{\bar{\tau}}_g = \varepsilon_g \mu_g (\nabla \vec{v}_g + \nabla \vec{v}_g^T) - \frac{2}{3} \varepsilon_g \mu_s \nabla \vec{v}_s \bar{\bar{\mathbf{I}}} \quad (3)$$

In the right-hand side of eq. (2), p is the pressure shared by all phases, $\bar{\bar{\tau}}_g$ – the g phase stress tensor, \vec{g} – the gravity acceleration $K(\vec{v}_s - \vec{v}_g)$ – the interaction force between phases, and K – the interphase momentum exchange coefficient.

In a similar manner, for a granular phase s , the conservation of momentum equation is:

$$\frac{\partial(\rho_s \varepsilon_s \vec{v}_s)}{\partial t} + \nabla(\rho_s \varepsilon_s \vec{v}_s \vec{v}_s) = -\varepsilon_s \nabla p_s + \nabla \bar{\bar{\tau}}_s + \varepsilon_s \rho_s \vec{g} + K(\vec{v}_g - \vec{v}_s) \quad (4)$$

In this equation, the terms, p_s , and $\bar{\bar{\tau}}_s$ are, respectively, the solid pressure and the solid shear stresses tensor. The difference between the eqs. (2) and (4) is the presence, in the eq. (4), of the solid-phase pressure, p_s , that represents the solid phase normal forces due to particle-particle interactions.

The expression for this term is the equation $p_s = \varepsilon_s \rho_s \Theta_s + 2\rho_s(1 + e_{ss})\varepsilon_s^2 g_{0,ss} \Theta_s$ proposed by Lun *et al.* Here e_{ss} is the restitution coefficient for particle collisions, Θ_s – the granular temperature, and $g_{0,ss}$ – the radial distribution function. The radial distribution function is used for measuring the probability of particle collisions and in the code the following equation is used:

$$g_{0,ss} = \left[1 - 3 \sqrt{\frac{\varepsilon_s}{\varepsilon_{s,max}}} \right]^{-1} \quad (5)$$

The solid shear stress tensor is $\bar{\bar{\tau}} = \varepsilon_s \mu_s (\nabla \bar{\bar{v}}_s + \nabla \bar{\bar{v}}_s^T) + \varepsilon_s (\lambda_s - 2/3 \mu_s) \nabla \bar{\bar{v}}_s \bar{\bar{I}}$. In this expression a shear and a bulk viscosity are present. Regarding the shear viscosity, the code considers a kinetic, a collision and, also, a frictional component to account for the viscous-plastic transition that occurs when particles of the solid phase reach a high value for solid volume fraction.

In the present simulations frictional stresses are not considered, so, the solid shear viscosity can be expressed as a sum of two terms as $\mu_s = \mu_{s,col} + \mu_{s,kin}$. We tested the Syamlal *et al.* [8] correlation and the Gidaspow correlation, that is:

$$\mu_s = \frac{4}{5} \varepsilon_s \rho_s d_s g_{0,ss} (1 + e_{ss}) \sqrt{\frac{\Theta_s}{\pi}} + \frac{10 \rho_s d_s \sqrt{\Theta_s} \pi}{96(1 + e_{ss}) g_{0,ss}} \left[1 + \frac{4}{5} (1 + e_{ss}) \varepsilon_s g_{0,ss} \right]^2 \quad (6)$$

The bulk viscosity which accounts for the resistance to compression and expansion of the granular particles is calculated with the well-known Lun *et al.* expression:

$$\lambda_s = \frac{4}{3} \varepsilon_s \rho_s d_s g_{0,ss} (1 + e_{ss}) \sqrt{\frac{\Theta_s}{\pi}} \quad (7)$$

The term Θ_s , granular temperature, accounts for the energy associated with the random fluctuating component of the particle velocity. The code uses the, generally accepted, kinetic theory of granular flow (KTGF), that permits to derive the stresses by the analogy between the random motion of a particle following a collision and the thermal agitation of molecules in a gas, taking into account the inelasticity of the granular phase. Thus, the fluid dynamic properties of the solid phase, such as the solid pressure and viscous force, can be described as a function of the granular temperature which can be expressed with a partial differential equation like the others transport equations. In the present investigation granular temperature was calculated with the algebraic formulation proposed by Syamlal *et al.* [8, 12]. It was demonstrated that, in case of dense fluidized bed [10], the use of the complete partial differential equation gives numerical predictions similar to those calculated with the algebraic equation.

Finally, regarding the phase interaction force, it is possible to choose between different models for the calculation of the fluid-solid exchange coefficient. In the simulations the Syamlal-O'Brien and the Gidaspow models were tested, however all the presented results refer to the second model and the interphase momentum exchange coefficient, K , is calculated with the equation:

$$K = 150 \frac{\varepsilon_s (1 - \varepsilon_g) \mu_g}{\varepsilon_g d_s^2} + 1.75 \frac{\varepsilon_s \rho_g}{d_s} |\bar{\bar{v}}_g - \bar{\bar{v}}_s| \quad (8)$$

Reference experimental set-up utilized in the numerical calculations

In recent years a biomass gasification plant was realized at ENEA. To study the fluid dynamics of the plant reactor a cold model was previously built. The method used for scaling-down the reactor and the procedure for the realization of the cold model are reported in [13-17]. In fig. 2 a sketch of this cold model is reported. The apparatus, divided in two chambers by the vertical plate, was made of Plexiglas containing, up to a certain height, the granular material. The wind-box was realized with stainless steel. Its architecture, in a dynamics similitude matter, reproduces the real biomass gasifier.

In according to similitude criteria, copper powder was recovered to simulate the gasifier bed material (silica sand). About 60 kg of copper powder were inserted inside the cold model. The height of the bed in minimal fluidizing condition was, approximately, equal to the sum of the height of separating plate (25 cm) and the height of the bottom orifice. Biomass was simulated with glass sphere of diameter equal to 2-2.5 mm. The air was injected at the bottom of the bed, but air was, also, introduced along the sloping wall, to avoid the formation of zones with poor fluidization and to account for the contribution due to devolatilization of the fuel in this zone of the real reactor. Injecting fluidizing air at different rates to the two chambers, two beds, interconnected by the bottom orifice, with different density are created. In these conditions, the main experimental tests performed with the cold model were:

- measure of the pressure difference between the two beds for various fluidization conditions by means of a metallic probe connected to a *U* tube manometer,
- visual observation of the solid particles and bubbles behaviour at different fluidization conditions,
- measure of circulation time of glass spheres at different fluidization conditions in the two beds by varying the orifice area of connection between the chambers at fixed fluidizing conditions, and
- calculation of the flux of the bed material across the orifice.

The complete results of the experimental tests regarding these phenomena can be found by Foscolo *et al.* [17]. In the present work a comparison between some of these experimental tests and simulation data is made. In particular, the comparison regards the fluidization quality, the bed behaviour at different regimes and the calculation of the flux of bed material across the orifice.

Numerical solution method

The computational grid, created with the CAD program GAMBIT™ 2.4.6, reproduces exactly, in a 2-D space, the dimensions and shape of the internal parts of the cold model. However, the top part of the freeboard is truncated to reduce the Cpu requested time for the simulations: this hypothesis does not modify the hydrodynamics behavior since the freeboard is high enough so that fully developed flow is observed. In fig. 3 one of the two grids used in the simulations is shown.

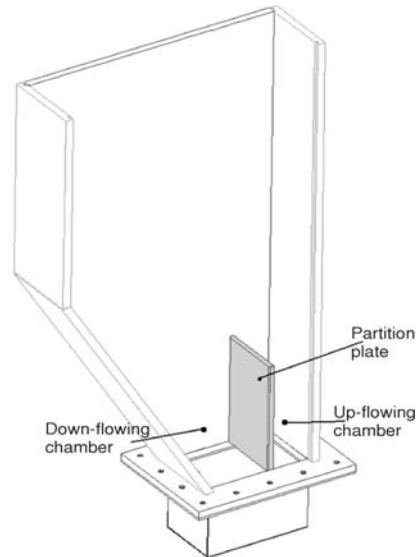


Figure 2. 3-D drawing of the cold model used in the experimental tests

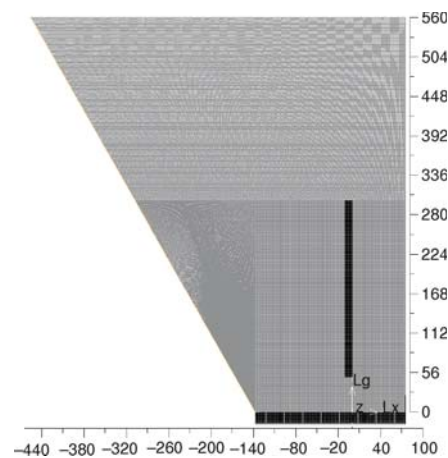


Figure 3. The 2-D grid used in the simulation with a 50 mm height bottom orifice

The grid is 212 mm wide at bottom and 525 mm at top, the total height is 578 mm. The vertical plate is 250 mm and the height of orifice is, in this case, equal to 50 mm (a similar grid with an orifice of 30 mm was also tested).

To account for the different fluid dynamics zones, for the bed and the freeboard different mesh regions, with different mesh spacing, were used. In certain fluidization conditions, the solid fell down across the distributor, so, some grid configurations with caps above the jets, to avoid loss of material, were proven. To reduce the problems of skewness (near the inclined wall) and of convergence, different conditions were tested. In particular, the grid dimensions were varied from 1 to 2 mm near the distributors and in the bottom part of the chambers, and from 2 to 4 mm in the freeboard. At the bottom of the bed a series of 2 mm gas jets allows the introduction of air. The nozzles of the up-flowing chamber are separated from those of the down-flowing chamber to separately manage the flows to be deployed in two chambers. At time zero, the fluid mesh regions in the bottom part of the grid, from the distributor up to the top line of the vertical plate, are filled with the granular material, considering a volume fraction less than the maximum solid packing fraction.

Table 1. Dimensions of the simulation grids and physical properties of the two phases

Geometric dimension	
– Height, [mm]	578
– Width	Variable with height
Settled bed height, H [mm]	300
Mean particles diameter, d_p [m]	122
Particles density, ρ_p [kgm^{-3}]	8822
Measured minimum fluidizing velocity, U_{mf} [ms^{-1}]	0.044
Measured bed voidage at U_{mf} , ϵ_{mf}	0.4
Fluid density, [kgm^{-3}]	1.2
Fluid viscosity, [$\text{Pa}\cdot\text{s}$]	1.8E-5

were used ($1.1 U_{mf}$ or $1.7 U_{mf}$) and, so, two different series of simulations were made. In each series, in the up-flowing chamber, superficial velocity was varied between $2.5 U_{mf}$ and $6.5 U_{mf}$. It is important to note that with these different fluidization conditions, different (very dense or dilute) regimes in the different regions of the bed can be created where both the kinetic and the frictional stresses can be dominant. However, in this work, as above mentioned, the frictional stresses are not considered.

The flow is modeled as being transient and, to capture the phenomena of interest, values between 0.00025 s to 0.0005 s were used for the time step. Turbulence of the gas phase is not considered.

The Phase Coupled SIMPLE (PC-SIMPLE) algorithm is used as pressure-velocity coupling and correction scheme and second order differencing schemes for momentum and volume fractions are used. The code runs in parallel mode on the ENEA-Cresco CPU-grid system.

In tab. 1 the geometric dimensions of the grid shown in fig. 3 and the physical parameters of the two phases are shown.

The IFB cold model is simulated in a 2-D domain in which there are no front and back wall effects. The walls were modeled using no slip boundary conditions. At the exit of freeboard a gauge pressure equal to 0 Pa is imposed. The influence of the particle-particle restitution coefficient on the hydrodynamics of bubbling beds and the measurement of the collision properties of spherical particles were investigated in many studies [18, 19], but no precise data for copper exist regarding these phenomena. In the present investigation the restitution coefficient was assumed equal to 0.95. At the inlet of the down-flowing chamber, two different velocities for the injected air

Computational results and comparison with experimental tests

Qualitative comparisons: fluidization quality and evidence of bed circulation

During cold model experimental testing, many conditions were explored (different superficial velocity, different height of orifice), and in all conditions, the quality of fluidization, the bubbles behavior and the bed expansion were visually analyzed. Furthermore the motion of the powder across the orifice was scanned as function of the superficial velocity. Figure 4 shows two images of the bed during a typical experimental test.



Figure 4. Pictures taken during the experimental tests by cold model

To analyze the quality of fluidization in the simulations, the volume fractions are considered. Figure 5 shows the contour plots, as function of time, of solid phase volume fraction of a typical result carried out using one of the explored fluidization conditions.

The images show the bubbles position from the beginning of the simulation until the burst of the bubbles at the top of the bed. It was observed the formation of large bubbles and that there is not a significant expansion of the bed before the formation of the bubbles in accordance to the fact that copper powder belongs to group B of Geldart classification [15, 20]. To investigate the formation and coalescing of each bubble during its rising in the

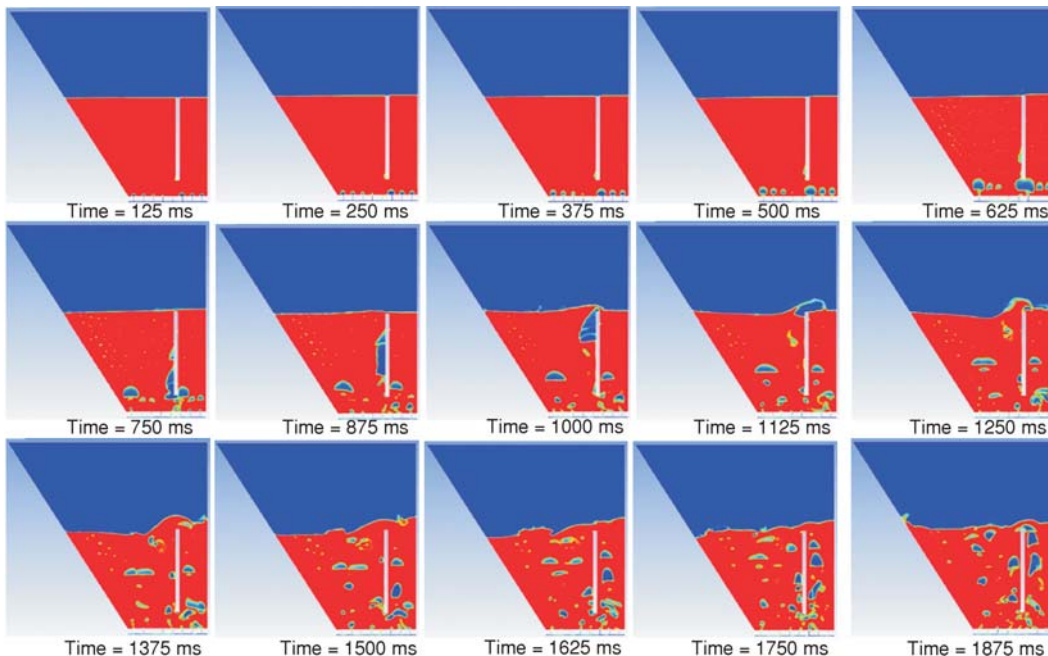


Figure 5. Solid phase volume fraction as function of time at $U_{DFB} = 1.1 U_{mf}$ and $U_{UFB} = 3 U_{mf}$, orifice height = 50 mm ($t = 125$ ms is the time interval between each snapshot)

right chamber the solid phase volume fraction was captured at every 125 ms at different U_{UFB} . For example, in fig. 6 the solid phase volume fractions at a fixed time $t = 2.5$ s, at different U_{UFB} , are plotted. The different growth of the bubbles is clearly observable and in particular it can be observed that for U_{UFB} greater than $3 U_{mf}$ the bubbles dimensions are very close to the width of right chamber.

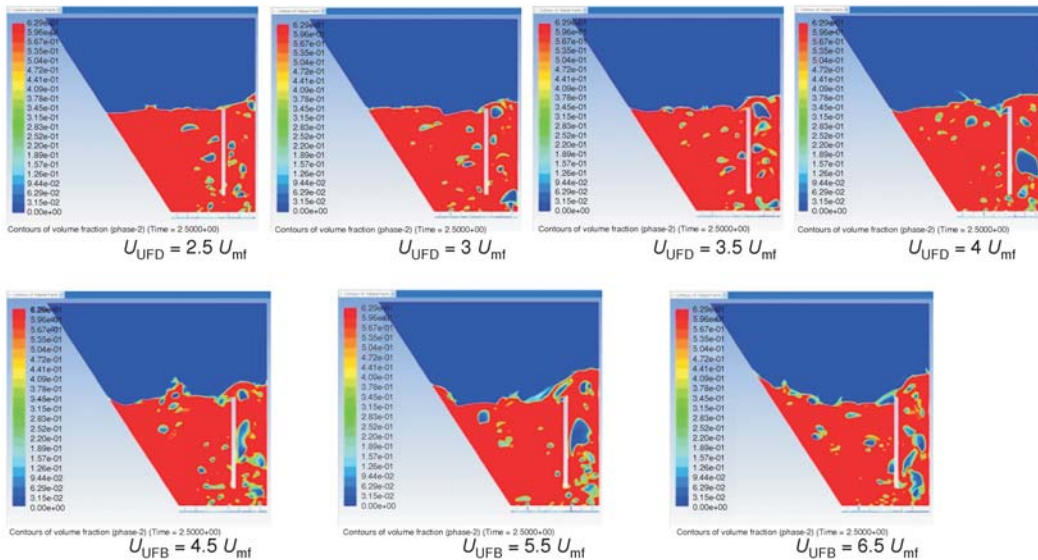


Figure 6. Solid phase volume fraction at time $t = 2.5$ s at different superficial velocity in the fast chamber; ($U_{DFB} = 1.1 U_{mf}$; $U_{UFB} = 2.5 U_{mf} - 6.5 U_{mf}$)

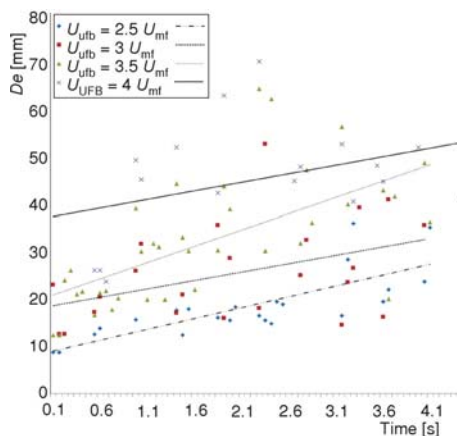


Figure 7. Equivalent diameter of the bubbles in the right chamber as function of time at four different U_{UFB} ($U_{DFB} = 1.1 U_{mf}$)

ter of bubbles grows up to a value higher than $2/3$ of the chamber linear dimension. These results fit well with experimental data of Foscolo *et al.*, who observed a transition from bubbling to slugging regime at an U_{UFB} value between $3 U_{mf}$ and $3.5 U_{mf}$ [17].

To determine the size of the bubbles in the right chamber, an equivalent average bubble diameter was calculated by averaging the bubble diameters: the bubble boundaries was defined as a void fraction greater than 0.85. Bubble diameter was calculated with the formula $De = (D_H D_V)^{1/2}$ [21-23], where D_H and D_V , represent the measured horizontal and vertical dimensions of a bubble. The calculated equivalent diameters for the bubbles in the up-flowing chamber are plotted in fig. 7 and an averaged value of the equivalent diameter and the maximum equivalent diameter, for the simulations with $U_{UFB} \leq 4 U_{mf}$, is reported in tab. 2. As expected both the average and maximum equivalent diameter have an increasing trend with U_{UFB} . It is interesting to observe that at $U_{UFB} \geq 3.5 U_{mf}$ the maximum diameter of bubbles

Table 2. Average equivalent diameter De , and maximum diameter, $\max De$, for the bubbles in the right chamber

	$U_{UFB} = 2.5 U_{mf}$	$U_{UFB} = 3 U_{mf}$	$U_{UFB} = 3.5 U_{mf}$	$U_{UFB} = 4 U_{mf}$
Average De [mm]	18	25	31	45
$\max De$ [mm]	35	52	64	71

To get information about the particles movement in the bed, the representations of the particles velocity vectors fields were analyzed every 62.5 ms. For example fig. 8 shows the instantaneous solid phase X-velocity fields at time $t = 3$ s.

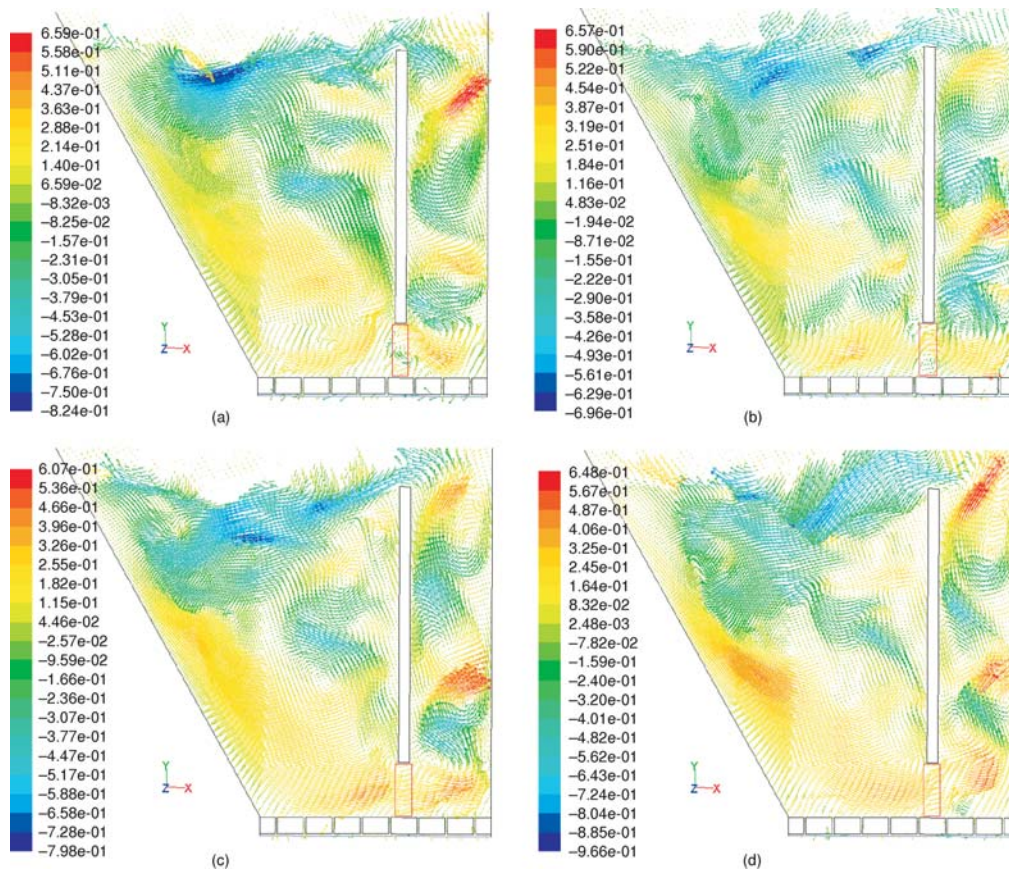


Figure 8. Particles X-velocity field at time $t = 3$ s; $U_{DFB} = 1.1 U_{mf}$ (a) $U_{UFB} = 2.5 U_{mf}$, (b) $U_{UFB} = 3 U_{mf}$, (c) $U_{UFB} = 3.5 U_{mf}$, (d) $U_{UFB} = 4 U_{mf}$

It is possible to note, in the left chamber, the vigorous movement of the particles, that ascend and descend in the bed generating vortices between the center and the walls. This type of motion (gulf stream circulation) is due to the bubbles that withdraw particles into their wakes and the subsequent creation of low and high bulk density regions that cause the rising and the fall of particles through the bed. In all four images the directions of the vectors in the regions below and above the partition plate indicate a counterclockwise circulation of the copper powder from the right chamber to the left one.

To analyze the superficial velocity dependence of the particles circulation a time-averaged value of the solid phase X-velocities was calculated in the orifice region below the partition plate (rectangles indicated in fig. 8) and, as forecasted, vectors magnitude increases as U_{UFB} increases (tab. 3).

Table 3. Time-averaged solid phase X-velocity in the region below the partition plate

	$U_{\text{UFB}} = 2.5 U_{\text{mf}}$	$U_{\text{UFB}} = 3 U_{\text{mf}}$	$U_{\text{UFB}} = 3.5 U_{\text{mf}}$	$U_{\text{UFB}} = 4 U_{\text{mf}}$
Averaged solid phase X-velocity [ms^{-1}]	0.022	0.097	0.116	0.15

All these observations confirm, qualitatively, the solid particles circulation observed in the experimental tests. In the next section, the flux per unit surface is calculated, and a quantitative comparison between the experimental data and simulation data is presented.

Quantitative comparison: flux across the orifice

A lot of experimental works can be found in literature to estimate the flow of particles through an orifice. Experimental correlations show that the mass solid flux across an orifice can be expressed applying a Bernoulli-type equation. So, in the cold model testing, to calculate the flux as function of the measured pressure difference across the two chambers, ΔP_0 , Foscolo *et al.* [17] used the eq. $W = C_{s0} \varepsilon_u^{2.35} (2\rho_d \Delta P_0)^{1/2}$ and, at $U_{\text{UFB}} = 3 U_{\text{mf}}$, they calculated a flux value of 470 $\text{kg/m}^2\text{s}$.

To compare this result with the numerical simulations, simulated data were recorded every 62.5 ms and, first of all, the mean bed voidage in the two chambers were calculated:

- $\overline{VF}_{\text{DFB}}$ mean bed voidage over the entire DFB domain (averaged between 2.5 to 5 s), and
- $\overline{VF}_{\text{UFB}}$ mean bed voidage over the entire UFB domain (averaged between 2.5 to 5 s).

Considering the hypothesis that, for Geldart B solids [20], voidage of emulsion can be approximated with the voidage at minimum fluidization, the average volume fraction of the bed in bubbles, can be calculated with formulas:

$$\delta_{\text{UFB}} = \frac{\overline{VF}_{\text{UFB}} - \varepsilon_{\text{mf}}}{1 - \varepsilon_{\text{mf}}} \quad \text{and} \quad \delta_{\text{DFB}} = \frac{\overline{VF}_{\text{DFB}} - \varepsilon_{\text{mf}}}{1 - \varepsilon_{\text{mf}}} \quad (9)$$

Then, calculating, for each simulation, the difference of volume fraction in bubbles between the two chamber, $\Delta\delta = \delta_{\text{UFB}} - \delta_{\text{DFB}}$, the graph in fig. 9(a) was obtained. As expected the difference increases with increasing of superficial velocity. The graph also shows that δ_{DFB} is not constant but slightly increases as U_{UFB} increases. This is due to the fact that, at greater U_{UFB} , the leakage of gas from the right chamber to the left one is higher than at low U_{UFB} and probably because the fluctuations of the bed overestimated the void fraction in the upper part of the left chamber.

So, averaged pressure difference between the two chambers is calculated with $\Delta P_0 = \Delta\delta(1 - \varepsilon_{\text{mf}})\rho_p gH$ and finally a time-averaged flux across the orifice can be calculated with the equation:

$$W = C_{s0} \varepsilon_u^{2.35} \sqrt{2\rho_d \Delta\delta(1 - \varepsilon_{\text{mf}})\rho_p gH} \quad (10)$$

The trend of flux W , as function of the ratio $U_{\text{UFB}}/U_{\text{mf}}$, is shown in fig. 9(b)

At $U_{\text{UFB}} = 3-3.5 U_{\text{mf}}$ the value of the flux is in the range of 400-430 $\text{kg/m}^2\text{s}$. These values, within the assumptions of the model, are very close to the values calculated in the cold

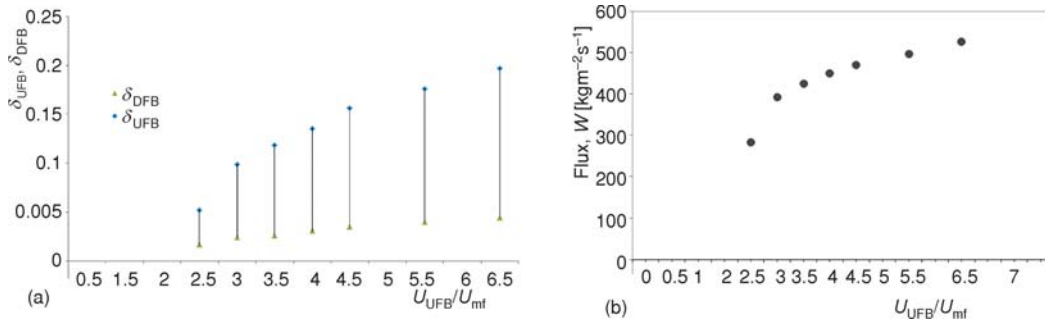


Figure 9. (a) Volume fraction in bubbles in the two chambers at different U_{UFB} , (b) Averaged solid mass flux; $U_{DFB}/U_{mf} = 1.1$, orifice height = 50 mm, $C_{s0} = 0.105$, $\varepsilon_u = 1$

model testing at the same conditions. Moreover the trend of the flux at different superficial velocity in the right chamber confirms that the quality and strength of the bed circulation depends on the difference of flow of gas sent into the two chambers.

Conclusions

The implemented 2-D model is capable of simulating the complex gas-solid flow behaviour in an interconnected bubbling fluidized bed. Within the assumed hypothesis, data confirmed that simulations can, qualitatively and quantitatively, well predict many of the features of the test rig. The following phenomena, observed in cold model testing, were also clearly observed in the simulations: the coalescence and rise of the bubbles, the circulation of the solid between the two chambers, the transition, in the fast chamber, from a bubbling fluidization regime to a slugging one.

Simulation data were used to calculate the flux of the solid material through the orifice, the calculated values of this latter fit well with the experimental tests. It can be concluded that the numerical model is a very valuable tool to study the hydrodynamic behaviour of the cold model and, using the scaling relations, to improve the fluidization quality of the bed inventory in the real reactor.

Acknowledgment

The authors would like to express their sincere thanks to Prof. Foscolo for his helpful suggestions.

Nomenclature

C_{s0} – particle discharge coefficient, [–]
 d_p – particle diameter, [m]
 De – equivalent diameter, [mm]
 D_H, D_V – bubble dimensions, [mm]
 e_{ss} – restitution coefficient for particles collision
 g – gravity acceleration constant, [ms^{-2}]
 $g_{0,ss}$ – radial distribution function, [–]
 H – height of the bed, [m]
 \mathbf{I} – unit tensor, [–]
 K – interphase momentum exchange coefficients, [$\text{kgm}^{-3}\text{s}^{-1}$]

ΔP_0 – pressure difference between the two chamber, [Pa]
 p – pressure, [Nm^{-2}]
 U – superficial gas velocity, [ms^{-1}]
 VF – void fraction
 v – velocity, [ms^{-1}]
 W – solid flux per unit area [$\text{kgm}^{-2}\text{s}^{-1}$]

Greek symbols

δ – bubble volumetric fraction
 ε – volume fraction
 ε_u – voidage at the bottom of UFB
 Θ_s – granular temperature, [m^2s^{-2}]

λ	– bulk viscosity, [$\text{kgm}^{-1}\text{s}^{-1}$]	DFB	– down-flowing bed
μ	– viscosity, [$\text{kgm}^{-1}\text{s}^{-1}$]	kin	– kinetic
ρ	– density, [kgm^{-3}]	mf	– minimum fluidization
ρ_d	– bed density at minimum fluidization, [kgm^{-3}]	q	– generic phase
$\bar{\tau}$	– stress tensor, [Nm^{-2}]	g, s	– fluid, solid phase
		UFB	– up-flowing bed

Subscripts

col – collisional

References

- [1] Kalina, J., Fossil Fuel Savings, Carbon Emission Reduction and Economic Attractiveness of Medium-Scale Integrated Biomass Gasification Combined Cycle Co-Generation Plants, *Thermal Science*, 16 (2012), 3, pp. 827-848
- [2] Gomez-Barea, A., Leckner, B., Modeling of Biomass Gasification in Fluidized Bed, *Progress in Energy and Combustion Science*, 36 (2010), 4, pp. 444-509
- [3] Kuramoto, M., *et al.*, Development of a New System for Circulating Fluidizing Particles within a Single Vessel, *Powder Technology*, 44 (1985), 1, pp. 77-84
- [4] Kuramoto, M., *et al.*, Flow of Dense Fluidized Particles through an Opening in a Circulation System, *Powder Technology*, 47 (1986), 2, pp. 141-149
- [5] Abellon, R. D., *et al.*, A Single Radiotracer Particle Method for the Determination of Solids Circulation Rate in Interconnected Fluidized Beds, *Powder Technology*, 92 (1997), 1, pp. 53-60
- [6] Snieders, F. F., *et al.*, The Dynamics of Large Particles in a Four-Compartment Interconnected Fluidized Bed, *Powder Technology*, 101 (1999), 3, pp. 229-239
- [7] Anderson, T. B., Jackson, R., *Fluid Mechanical Description of Fluidized Beds. Equations of Motion – Industrial & Engineering Chemistry Fundamentals* (ACS Publications), 1967
- [8] Syamlal, M., *et al.*, MFIX Documentation: Theory Guide, Tech. Note, NTIS Report No. DOE/METC-94/1004 (DE94000087) Springfield, Va., USA
- [9] Enwald, H., *et al.*, Eulerian Two-Phase Flow Theory Applied to Fluidization, *Int. J. Multiphase Flow*, 22 (1996), Suppl., pp. 21-66
- [10] Boemer, A., *et al.*, Eulerian Simulation of Bubble Formation at a Jet in a Two-Dimensional Fluidized Bed, *Int. J. Multiphase Flow*, 23 (1997), 5, pp. 927-944
- [11] Reuge, N., *et al.*, Multifluid Eulerian Modeling of Dense Gas-Solids Fluidized Bed Hydrodynamics: Influence of the Dissipation Parameters *Chemical Engineering Science*, 63 (2008), 22, pp. 5540-5551
- [12] ***, FLUENT User's Guide. FLUENT Inc. 2009
- [13] Glicksman, L. R., Scaling Relationships for Fluidized Beds, *Chemical Engineering Science*, 39 (1984), 9, pp. 1373-1379
- [14] Kunii, D., Levenspiel, O., *Fluidization Engineering*, 2nd edn. Butterworth-Heinemann, Boston, Mass., USA, 1991
- [15] Gibilaro, L. G., *Fluidization-Dynamics*, Butterworth Heinemann, Oxford, UK, 2001
- [16] Di Felice, R., *et al.*, Dynamic Similarity Rules: Validity Check for Bubbling and Slugging Fluidized Beds, *Powder Technology*, 71 (1992), pp. 281-287
- [17] Foscolo, P. U., *et al.*, Design and Cold Model Testing of a Biomass Gasifier Consisting of Two Interconnected Fluidized Beds, *Powder Technology*, 173 (2007), 3, pp. 179-188
- [18] Foerster, S. F., *et al.*, Measurements of the Collision Properties of Small Spheres, *Phys. Fluids*, 6 (1994), 3, pp. 1108-1115
- [19] ***, Cornell University College of Engineering, <http://grainflowresearch.mae.cornell.edu>
- [20] Geldart, D., Types of Gas Fluidization, *Powder Technology*, 7 (1973), 5, pp. 285-292
- [21] van Wachem, B. G. M., *et al.*, Eulerian Simulations of Bubbling Behaviour in Gas-Solid Fluidised Beds, *Computers Chem. Eng.*, 22 (1998), Suppl., pp. S299-S306
- [22] Hulme, I., *et al.*, CFD Modeling and Validation of Bubble Properties for a Bubbling Fluidized Bed Ind., *Eng. Chem. Res.*, 44 (2005), 12, pp. 4254-4266
- [23] Kuipers, J. A.M., *et al.*, Theoretical and Experimental Bubble Formation at a Single Orifice in a Two-Dimensional Gas-Fluidized Bed, *Chemical Engineering Science*, 46 (1991), 1 I, pp. 2881-2894

Paper submitted: December 20, 2012

Paper revised: December 20, 2013

Paper accepted: December 20, 2013